Commun. Comput. Phys.
doi: 10.4208/cicp.250910.131011a

Vol. **12**, No. 4, pp. 955-980
October 2012

An All-Speed Asymptotic-Preserving Method for the Isentropic Euler and Navier-Stokes Equations

Jeffrey Haack[1,2,*], Shi Jin[1] and Jian-Guo Liu[3]

[1] *Department of Mathematics, University of Wisconsin-Madison, Madison, WI 53706, USA.*
[2] *Department of Mathematics, University of Texas at Austin, Austin, TX 78712, USA.*
[3] *Departments of Physics and Mathematics, Duke University, Durham, NC 27708, USA.*

Received 25 September 2010; Accepted (in revised version) 13 October 2011

Available online 28 March 2012

Abstract. The computation of compressible flows becomes more challenging when the Mach number has different orders of magnitude. When the Mach number is of order one, modern shock capturing methods are able to capture shocks and other complex structures with high numerical resolutions. However, if the Mach number is small, the acoustic waves lead to stiffness in time and excessively large numerical viscosity, thus demanding much smaller time step and mesh size than normally needed for incompressible flow simulation. In this paper, we develop an all-speed asymptotic preserving (AP) numerical scheme for the compressible isentropic Euler and Navier-Stokes equations that is uniformly stable and accurate for all Mach numbers. Our idea is to split the system into two parts: one involves a slow, nonlinear and conservative hyperbolic system adequate for the use of modern shock capturing methods and the other a linear hyperbolic system which contains the stiff acoustic dynamics, to be solved implicitly. This implicit part is reformulated into a standard pressure Poisson projection system and thus possesses sufficient structure for efficient fast Fourier transform solution techniques. In the zero Mach number limit, the scheme automatically becomes a projection method-like incompressible solver. We present numerical results in one and two dimensions in both compressible and incompressible regimes.

AMS subject classifications: 35Q35, 65M08, 65M99, 76M12, 76N99

Key words: Low Mach number limit, asymptotic preserving schemes, incompressible limit, projection scheme, isentropic Euler equation.

*Corresponding author. *Email addresses:* haack@math.utexas.edu (J. Haack), jin@math.wisc.edu (S. Jin), jian-guo.liu@duke.edu (J.-G. Liu)

1 Introduction

We are interested in the efficient numerical simulation of unsteady compressible flows with all range of Mach numbers. These flows arise in many physical applications, including atmospheric modeling, magnetohydrodynamics and combustion. When the Mach number is of order one, modern shock capturing methods provide high resolution numerical approximations to shocks and other complex flow structures. However, when the Mach number is small, near the so-called incompressible regime, there is a wide gap between the speeds of the flow and the acoustic waves, the latter of which is often unimportant in the incompressible regime. In the incompressible regime, standard explicit shock-capturing methods require the time step to scale inversely with the maximum wave speed in the system for stability, which greatly *overresolves the solution in time*. Furthermore, these shock capturing methods will introduce numerical diffusions that scale with the inverse of the wave speeds around discontinuities, which requires *overresolution in space* in order to ensure that the numerical diffusion does not dominate the solution or physical viscosity for high Reynolds number flows.

Our goal is to develop all-speed flow simulators that work in all regimes of Mach number, including both compressible and incompressible regimes and their mixture. As a first step, in this paper, we focus on the compressible isentropic Euler and Navier-Stokes equations of gas dynamics. It was shown by Klainerman and Majda [23] that solutions to these equations converge to solutions of the incompressible equations in the limit when the Mach number goes to zero. The major difference between compressible and incompressible systems lies in the pressure term. In the compressible case, the pressure is determined by the equation of state of the system and plays an important role in the flux terms of the conservation law and is the source of the acoustic waves in the system. However, in the limiting incompressible equations the pressure term acts as a Lagrange multiplier to enforce the incompressibility condition and is in fact an asymptotic perturbation of the physical pressure from the compressible equations.

The development of computational methods for nearly incompressible (small Mach number flows) has attracted great attention for many years. Much of the early literature in this area focused on preconditioning techniques for steady state problems. In fact, Chorin's artificial compressibility approach [4] sought to avoid the difficulties of the pressure term in the incompressible equations by solving a form of the compressible low Mach number system, which has much clearer boundary conditions. It was later recognized [31] that these ideas could be used to calculate steady states of incompressible flows. Later studies applied these ideas to compute solutions to low Mach number flow by introducing preconditioning matrices to symmetrize the system in terms of a set of non-conservative variables [1, 14]. However, these methods assume that the flow is already in the low Mach number regime and thus cannot accurately compute problems where the Mach number is of order unity. Guillard and Viozat [13] followed the asymptotic analysis of Klainerman and Majda [23] to show that the artificial numerical dissipation in upwind methods for the Euler equation are what causes the method to

perform poorly in the low Mach number limit and use the preconditioner of Turkel [31] to alter the dissipation terms in their method to capture the correct limit. Colella and Pao [5] used the Hodge decomposition to split the method into incompressible and irrotational components and obtained a method that is applicable to the broader regime of flows with Mach number less than one. However, the accuracy breaks down at the higher Mach numbers and it does not capture the correct speeds of the acoustic waves in regimes where they become important. This work was later extended by Gatti-Bono and Colella in the context of atmospheric flows [11].

Other approaches have sought to develop all-speed methods, which are suited to both fully compressible and low Mach number regimes. Harlow and Amsden [15] sought to extend the staggered-mesh MAC scheme for incompressible flows [16] to compressible flows. Their method, the Implicit Continuous-fluid Eulerian (ICE) method, iteratively solves an implicit second-order wave equation to update the density and pressure terms. However, this scheme is not conservative and has difficulties in capturing strong shocks. Inspired by this work, Degond and Tang [8] split the stiff pressure term with a numerical parameter to derive a nonlinear elliptic equation for the density updates that acts similarly to a classical incompressible projection on the system. Klein [24] presents a predictor-corrector type method based on pressure variables at each order in the asymptotic expansion of the pressure. Kadioglu et al. [21] developed a method using a second order preconditioner algorithm that captured the correct shock speed and suppressed oscillations in multi-fluid systems. However, in low Mach regimes this method still requires temporal resolution of the Mach number for stability.

In this paper, we present a new numerical method for the solution of the isentropic Euler and Navier-Stokes equations that is valid for all Mach numbers (namely the *all-speed* property). It allows the use of standard conservative shock capturing methods that are necessary for the compressible regime, yet the method is shown to be *Asymptotic Preserving (AP)* [17] in the zero Mach number limit. An Asymptotic Preserving method is a method that preserves, at the discrete level, the asymptotic passage from one model to another. Specifically, if the time and spatial steps Δt and Δx are kept fixed, as the small scale parameter goes to zero, the method automatically transforms to a stable discretization of the limiting model. In our case here, the limiting scheme, when the Mach number goes to zero, becomes a good incompressible solver similar to a second order projection method. By adequately splitting the compressible Euler/Navier-Stokes equations into a compressible, non-stiff nonlinear hyperbolic system and a stiff linear acoustic wave system which can be easily handled by a fast Fourier transform based Poisson solver, our method allows the use of sound speed (essentially the reciprocal of the Mach number) independent time and spatial steps.

The asymptotic-preserving approach was first introduced in the context of linear transport in diffusive regimes [12, 19, 26] and have since been extended to many other areas such as fluid and diffusion limits of kinetic models and relaxation methods for hyperbolic systems. In [7], Degond, Jin and Liu studied the time discretization of Asymptotic Preserving methods for several compressible flow problems by means of a Hodge-like

decomposition. While our work was inspired by this research, we capture the low Mach number limit in a different fashion.

Our paper is organized as follows. In Section 2, we review the details of the low Mach number limit of the isentropic Euler equations and make a close study of the difficulties encountered by standard hyperbolic shock capturing methods in this regime. In Section 3 we propose a hyperbolic splitting of the system to separate the fast acoustic waves from the low-speed hyperbolic flow. The fast acoustic system is a linear hyperbolic system with constant coefficients, which can be solved implicitly, while the relatively slow system contains the flow dynamics and is solved using an explicit shock capturing central scheme. We then perform an asymptotic analysis to show that the scheme becomes an incompressible scheme in the low Mach number limit. In Section 4 we provide numerical results on a number of problems in both compressible and incompressible regimes and the paper is concluded in Section 5.

2 Low Mach number limit of the isentropic Navier-Stokes equations

The isentropic Navier-Stokes equations in general spatial dimension are given by

$$\begin{aligned}&\rho_t+\nabla\cdot(\rho\mathbf{u})=0,\\&(\rho\mathbf{u})_t+\nabla\cdot(\rho\mathbf{u}\otimes\mathbf{u})+\nabla p(\rho)=\mu\Delta\mathbf{u},\\&p(\rho)=A\rho^\gamma.\end{aligned}$$

Here, ρ is the density of the fluid, $\mathbf{m}=\rho\mathbf{u}$ is the momentum of the fluid, μ is the dynamic viscosity of the fluid and $p(\rho)$ is the pressure. Typically air is composed of N_2 and O_2, which gives $\gamma=1.4$ and we take $A=1$ for simplicity. One can also obtain the shallow water equations by setting $\gamma=2$ and $A=g/2$. To obtain the Euler equations, set $\mu=0$.

To describe the low Mach number (incompressible) limit, one scales the equations in the following manner. Let x_0, t_0, ρ_0, p_0, u_0 be a set of characteristic scales for the variables in the equations. The dimensionless variables are then given by $\hat{x}=x/x_0$, $\hat{t}=t/t_0$, etc. Inserting these into the equations (and dropping the hats), one obtains the nondimensionalized equations

$$\begin{aligned}&\frac{\rho_0}{t_0}\rho_t+\frac{\rho_0u_0}{x_0}\nabla\cdot(\rho\mathbf{u})=0,\\&\frac{\rho_0u_0}{t_0}(\rho\mathbf{u})_t+\frac{u_0^2\rho_0}{x_0}\nabla\cdot(\rho\mathbf{u}\otimes\mathbf{u})+\frac{p_0}{x_0}\nabla p=\frac{u_0\mu}{x_0^2}\Delta\mathbf{u},\\&p_0p=\rho_0^\gamma\rho^\gamma.\end{aligned}$$

Using the fact that $u_0=x_0/t_0$, one has

$$\rho_t+\nabla\cdot(\rho\mathbf{u})=0,$$

$$(\rho\mathbf{u})_t+\nabla\cdot(\rho\mathbf{u}\otimes\mathbf{u})+\frac{p_0}{\rho_0u_0^2}\nabla p=\frac{1}{\mathrm{Re}}\Delta\mathbf{u},$$
$$\frac{p_0}{\rho_0^\gamma}p(\rho)=\rho^\gamma.$$

Here $\mathrm{Re}=\rho_0u_0x_0/\mu$ is the dimensionless Reynolds number, which measures the ratio between the inertial and diffusive forces in the system. p_0 scales as ρ_0^γ, as expected from the equation of state. What remains to be determined is the term in front of the pressure. Since the speed of sound is given by $c^2=\gamma p/\rho$, one has $c_0^2c^2=\gamma p_0p/\rho_0\rho$ and thus one defines the dimensionless reference Mach number to be $\varepsilon^2=\gamma u_0^2/c_0^2=\rho_0u_0^2/p_0$. The nondimensionalized equations then take the form

$$\rho_t+\nabla\cdot(\rho\mathbf{u})=0, \tag{2.1a}$$
$$(\rho\mathbf{u})_t+\nabla\cdot(\rho\mathbf{u}\otimes\mathbf{u})+\frac{1}{\varepsilon^2}\nabla p=\frac{1}{\mathrm{Re}}\Delta\mathbf{u}, \tag{2.1b}$$
$$p=\rho^\gamma. \tag{2.1c}$$

2.1 The low Mach number limit

To determine the asymptotic behavior as $\varepsilon\to0$, one takes an asymptotic expansion of the variables as

$$\rho=\rho^{(0)}+\varepsilon^2\rho^{(2)}+\cdots,$$

for small ε and look at the balances within the equations. At $\mathcal{O}(\varepsilon^{-2})$, one has the balance

$$\nabla p^{(0)}=0\ \Rightarrow\ p^{(0)}(\mathbf{x},t)=p^{(0)}(t)\ \Rightarrow\ \rho^{(0)}=\rho^{(0)}(t),$$

i.e., the leading order pressure (and hence density) are constant in space.

Next, use this fact to enforce incompressibility. The $\mathcal{O}(1)$ equations are

$$\partial_t\rho^{(0)}+\nabla\cdot(\rho^{(0)}\mathbf{u}^{(0)})=0, \tag{2.2}$$
$$\partial_t(\rho^{(0)}\mathbf{u}^{(0)})+\nabla\cdot(\rho^{(0)}\mathbf{u}^{(0)}\otimes\mathbf{u}^{(0)})+\nabla p^{(2)}=0. \tag{2.3}$$

Incompressibility is enforced using the *boundary conditions*. Three types of boundary conditions that give incompressibility are listed below.

1. **Wall boundary condition**. The problem takes place in a bounded domain Ω with fixed walls. In this case $\mathbf{u}\cdot n=0$ on $\partial\Omega$. Thus, if one integrates the density equation over the domain one obtains

$$|\Omega|\partial_t\rho^{(0)}+\rho^{(0)}\int_\Omega\nabla\cdot\mathbf{u}^{(0)}=0,\qquad \partial_t\rho^{(0)}=-\frac{\rho^{(0)}}{|\Omega|}\int_\Omega\nabla\cdot\mathbf{u}^{(0)},$$
$$\partial_t\rho^{(0)}=-\frac{\rho^{(0)}}{|\Omega|}\int_{\partial\Omega}\mathbf{u}^{(0)}\cdot n,\qquad \partial_t\rho^{(0)}=0.$$

The last step comes from applying the boundary condition. Thus the density does not change and one sets $\nabla\cdot\mathbf{u}^{(0)}=0$.

2. **Periodic boundary condition**. This result is similar to the above. Integrating over the domain gives

$$|\Omega|\partial_t\rho^{(0)}+\rho^{(0)}\int_\Omega\nabla\cdot\mathbf{u}^{(0)}=0, \qquad \partial_t\rho^{(0)}=-\frac{\rho^{(0)}}{|\Omega|}\int_\Omega\nabla\cdot\mathbf{u}^{(0)},$$
$$\partial_t\rho^{(0)}=-\frac{\rho^{(0)}}{|\Omega|}\int_{\partial\Omega}\mathbf{u}^{(0)}\cdot n, \qquad \partial_t\rho^{(0)}=0.$$

The last step cancels out because the velocities are the same at opposite ends of the box, while the normal vectors point in opposite directions, thus giving the cancelation. Again one gets that $\nabla\cdot\mathbf{u}^{(0)}=0$.

3. **Open boundary.** In this case, one needs to have some sort of far-field boundary condition–usually this is enforced on the pressure. By assuming that this does not change with time (which makes sense, as it is just a general background pressure), one gets that $P^{(0)}(t)=P_0=\rho^{(0)}$ and thus $\partial_t\rho^{(0)}=0$, giving $\nabla\cdot\mathbf{u}^{(0)}=0$.

One consequence of these results is that incompressibility comes from a *global* procedure–a numerical scheme that hopes to capture it will have to take this into account.

Thus, assuming one of these boundary conditions one has that $\rho^{(0)}$ is constant in space and time and the incompressibility condition is satisfied for the leading order velocity. Next, looking at the $\mathcal{O}(1)$ momentum equation

$$\rho^{(0)}\partial_t\mathbf{u}^{(0)}+\rho^{(0)}\nabla\cdot(\mathbf{u}^{(0)}\otimes\mathbf{u}^{(0)})+\nabla p^{(2)}=\frac{1}{\mathrm{Re}}\Delta\mathbf{u}^{(0)},$$

using the incompressibility found above gives

$$\nabla\cdot\mathbf{u}^{(0)}=0,$$
$$\partial_t\mathbf{u}^{(0)}+(\mathbf{u}^{(0)}\cdot\nabla)\mathbf{u}^{(0)}+\frac{1}{\rho^{(0)}}\nabla p^{(2)}=\frac{1}{\mathrm{Re}}\Delta\mathbf{u}^{(0)},$$

which is the incompressible Navier-Stokes equation.

2.2 Numerical difficulties in the low Mach number limit

Standard finite volume shock-capturing hyperbolic solvers have difficulties in the low Mach number regimes. The compressible equations have acoustic waves that scale as $\mathcal{O}(\varepsilon^{-1})$ which require temporal resolution for stability. Furthermore, artificial viscosity on the order of the wave speeds is also introduced to suppress numerical oscillations across shocks and contact discontinuities. Thus, for a desired spatial accuracy, one must

also resolve the waves in space. This is prohibitively expensive to undertake as the underlying incompressible system does not admit these acoustic waves and the relevant time scale of interest is that of the fluid velocity $\mathbf{u}$. We illustrate these problems by looking at the one-dimensional Euler system with a simple local Lax-Friedrichs finite volume method, for simplicity, though the same issues will arise with other standard choices for the numerical flux

$$\begin{aligned}
&\frac{\rho_j^{n+1}-\rho_j^n}{\Delta t}+\frac{m_{j+1}^n-m_{j-1}^n}{2\Delta x}-\frac{\lambda_{j+\frac{1}{2}}}{2\Delta x}(\rho_{j+1}^n-\rho_j^n)+\frac{\lambda_{j-\frac{1}{2}}}{2\Delta x}(\rho_j^n-\rho_{j-1}^n)=0,\\
&\frac{m_j^{n+1}-m_j^n}{\Delta t}+\frac{(m^2/\rho)_{j+1}^n-(m^2/\rho)_{j-1}^n}{2\Delta x}+\frac{1}{\varepsilon^2}\frac{p_{j+1}^n-p_{j-1}^n}{2\Delta x}\\
&\qquad-\frac{\lambda_{j+\frac{1}{2}}}{2\Delta x}(m_{j+1}^n-m_j^n)+\frac{\lambda_{j-\frac{1}{2}}}{2\Delta x}(m_j^n-m_{j-1}^n)=0.
\end{aligned}$$

Here $\lambda_{j+1/2}=\max\{\lambda_j,\lambda_{j+1}\}$, where λ_j is the maximum wave speed based on the values in cell j.

The maximum wave speed of the system is $\lambda_{\max}=|u_{\max}|\pm\varepsilon^{-1}\sqrt{p'(\rho_{\max})}$ (where $u_{\max}$ and $\rho_{\max}$ are the values at the point where the maximum wave speed is reached); thus one needs

$$\Delta t=\nu\frac{\Delta x}{\lambda_{\max}}=\nu\frac{\Delta x\varepsilon}{\varepsilon|u_{\max}|+\sqrt{p'(\rho_{\max})}}=\mathcal{O}(\varepsilon\Delta x)$$

for some $0\leq\nu\leq 1$ to satisfy the CFL condition for stability. Furthermore, the numerical diffusion, while local, will at least at one point be given by

$$\frac{\Delta x\lambda_{\max}}{2}=\frac{\Delta x}{\varepsilon}\frac{(\varepsilon|u_{\max}|+\sqrt{p'(\rho_{\max})})}{2\nu}.$$

Thus one needs $\Delta x=o(\varepsilon)$ for accuracy purposes, ensuring that the numerical diffusion does not dominate the solution. A further consequence of this is that one now needs $\Delta t=o(\varepsilon\Delta x)=o(\varepsilon^2)$. This is unacceptable, as the limiting incompressible equations only have a timestep restriction of $\Delta t=\mathcal{O}(\Delta x)$, independent of ε.

3 The all-speed asymptotic-preserving method for the isentropic Navier-Stokes equations

3.1 All-speed asymptotic-preserving schemes

Our goal is to develop a method that preserves, at the discrete level, the asymptotic passage from the compressible equations to the incompressible equations *without* resolving the spatial and temporal scales associated with the acoustic waves, which are unimportant in the limit. In particular, the numerical method should demonstrate this discrete asymptotic limit by *being consistent* with a method for the incompressible equations in

the low Mach number limit. This discrete limit is taken with *spatial and temporal steps fixed*, with only the reference Mach number parameter driven to zero. A method that satisfies these properties is said to be asymptotic-preserving (AP) [17].

We stress that we want to obtain an *all-speed* scheme, in other words, a scheme that gives correct solutions for any reference Mach number ε, not just in the low Mach number regime. Therefore, we need to construct a scheme robust for all regimes. To this end, we work in *conservative variables*, to ensure that the scheme can capture shocks in the compressible regimes, (i.e., Mach number of order unity). On the other hand, incompressible solvers typically have an implicit global projection step that calculates an intermediate velocity field and pressure to update the velocity equations. This suggests that our overall scheme should be semi-implicit, weaving together these features of the two systems.

3.2 A hyperbolic splitting

Looking at the compressible system (2.1), there are two scales that we need to resolve: the (fast) acoustic wave scale and the (slow) convection scale, which contains the underlying incompressible dynamics. Therefore, we split the system into two systems. First, write the N-S equations as

$$\partial_t\rho+\alpha\nabla\cdot(\rho\mathbf{u})+(1-\alpha)\nabla\cdot(\rho\mathbf{u})=0, \tag{3.1a}$$

$$\partial_t(\rho\mathbf{u})+\nabla\cdot(\rho\mathbf{u}\otimes\mathbf{u})+\nabla\Big(\frac{p(\rho)-a(t)\rho}{\varepsilon^2}\Big)+\frac{a(t)}{\varepsilon^2}\nabla\rho=\frac{1}{\mathrm{Re}}\Delta\mathbf{u}. \tag{3.1b}$$

The slow dynamics evolves according to the system

$$\partial_t\rho+\alpha\nabla\cdot(\rho\mathbf{u})=0, \tag{3.2a}$$

$$\partial_t(\rho\mathbf{u})+\nabla\cdot(\rho\mathbf{u}\otimes\mathbf{u})+\nabla\Big(\frac{p(\rho)-a(t)\rho}{\varepsilon^2}\Big)=\frac{1}{\mathrm{Re}}\Delta\mathbf{u} \tag{3.2b}$$

and the fast dynamics is governed by the system

$$\partial_t\rho+(1-\alpha)\nabla\cdot(\rho\mathbf{u})=0, \tag{3.3a}$$

$$\partial_t(\rho\mathbf{u})+\frac{a(t)}{\varepsilon^2}\nabla\rho=0. \tag{3.3b}$$

The key idea is to split the stiff pressure term. We subtract off a linear piece $a(t)\rho$, to be determined below and add it back in fast system. The splitting parameter $0<\alpha<1$ determines how much of the momentum is seen by each system. As we will see, some momentum is necessary in the fast system to ensure incompressibility.

The choice of the splitting parameter $a(t)$ is motivated by hyperbolicity. In the two-dimensional case, for example, the wave speeds of (3.2) in the x direction are

$$\lambda=u,u\pm\sqrt{(1-\alpha)u^2+\frac{\alpha(p'(\rho)-a(t))}{\varepsilon^2}},$$

where u is the first component of $\mathbf{u}$, so if we choose

$$a(t)=\min_{\mathbf{x}} p'(\rho)$$

for our pressure splitting term, we ensure that the wave speeds will always be real and thus the slow system is hyperbolic. As we will see in the asymptotic analysis later, in the low Mach number limit the fast system (3.3) will force variations in ρ to be small and thus the wave speeds of the slow system will be $\mathcal{O}(1)$. We can discretize this system using any shock-capturing hyperbolic solver, noting that the wave speeds are no longer stiff which avoids the dissipation and time step problems seen in the original system (2.1). The fast dynamics, contained in (3.3), are simply a linear hyperbolic system with constant coefficients, which leads to a straightforward implicit implementation.

3.3 Time discretization of the split systems

For a first order in time scheme, we can write the system in a simple semi-implicit form

$$\frac{\rho^{n+1}-\rho^n}{\Delta t}+\alpha\nabla\cdot(\rho\mathbf{u})^n+(1-\alpha)\nabla\cdot(\rho\mathbf{u})^{n+1}=0, \tag{3.4a}$$

$$\frac{(\rho\mathbf{u})^{n+1}-(\rho\mathbf{u})^n}{\Delta t}+\nabla\cdot(\rho\mathbf{u}\otimes\mathbf{u})^n+\nabla\Big(\frac{p(\rho)-a(t)\rho}{\varepsilon^2}\Big)^n+\frac{a(t)}{\varepsilon^2}\nabla\rho^{n+1}=\frac{1}{\mathrm{Re}}\Delta\mathbf{u}^n. \tag{3.4b}$$

To obtain second order in time, we use a two-level Adams-Bashforth discretization for the explicit, slow terms and Crank-Nicholson for the fast, implicit terms

$$\frac{\rho^{n+1}-\rho^n}{\Delta t}+\alpha\nabla\cdot\Big(\frac{3}{2}(\rho\mathbf{u})^n-\frac{1}{2}(\rho\mathbf{u})^{n-1}\Big)+(1-\alpha)\nabla\cdot\Big(\frac{(\rho\mathbf{u})^{n+1}+(\rho\mathbf{u})^n}{2}\Big)=0, \tag{3.5a}$$

$$\begin{aligned}&\frac{(\rho\mathbf{u})^{n+1}-(\rho\mathbf{u})^n}{\Delta t}+\nabla\cdot\Big(\frac{3}{2}(\rho\mathbf{u}\otimes\mathbf{u})^n-\frac{1}{2}(\rho\mathbf{u}\otimes\mathbf{u})^{n-1}\Big)+\nabla\frac{3}{2}\Big(\frac{p(\rho)-a(t)\rho}{\varepsilon^2}\Big)^n\\&\quad-\frac{1}{2}\nabla\Big(\frac{p(\rho)-a(t)\rho}{\varepsilon^2}\Big)^{n-1}+\frac{a(t)}{\varepsilon^2}\nabla\frac{\rho^{n+1}+\rho^n}{2}=\frac{1}{\mathrm{Re}}\Delta\Big(\frac{3}{2}\mathbf{u}^n-\frac{1}{2}\mathbf{u}^{n-1}\Big).\end{aligned} \tag{3.5b}$$

Degond and Tang [8] noted that one can rewrite the momentum equation in (3.5b) in terms of $(\rho\mathbf{u})^{n+1}$ and insert it into the density equation, obtaining an elliptic equation for ρ^{n+1}:

$$\begin{aligned}&\frac{\rho^{n+1}-\rho^n}{\Delta t}+\alpha\nabla\cdot\Big(\frac{3}{2}(\rho\mathbf{u})^n-\frac{1}{2}(\rho\mathbf{u})^{n-1}\Big)+(1-\alpha)\Delta t\nabla\cdot(\rho\mathbf{u})^n\\&\quad-\frac{(1-\alpha)\Delta t}{2}\nabla\cdot\nabla\cdot\Big(\frac{3}{2}(\rho\mathbf{u}\otimes\mathbf{u})^n-\frac{1}{2}(\rho\mathbf{u}\otimes\mathbf{u})^{n-1}\Big)\\&\quad-\frac{(1-\alpha)\Delta t}{2}\nabla\cdot\nabla\Big(\frac{3}{2}\Big(\frac{p(\rho)-a(t)\rho}{\varepsilon^2}\Big)^n-\frac{1}{2}\Big(\frac{p(\rho)-a(t)\rho}{\varepsilon^2}\Big)^{n-1}\Big)\\&\quad-\frac{(1-\alpha)\Delta t}{2}\nabla\cdot\frac{a(t)}{\varepsilon^2}\nabla\frac{\rho^{n+1}+\rho^n}{2}=\frac{(1-\alpha)\Delta t}{2}\Delta\Big(\frac{3}{2}\nabla\cdot\mathbf{u}^n-\frac{1}{2}\nabla\cdot\mathbf{u}^{n-1}\Big).\end{aligned} \tag{3.6}$$

This system is now a Helmholtz equation for the unknown variable ρ^{n+1} and the terms from the previous steps can be pushed to the right hand side as source terms. If the right spatial discretization is chosen, this system can be solved efficiently for ρ^{n+1} using Fast Fourier Transform techniques. An important feature of this Helmholtz equation is that it is uniformly elliptic for any ε [6,9]. The updated momentum $(\rho^{n+1}\mathbf{u}^{n+1})$ is then obtained from the momentum equation (3.5b).

Note that, while popular in many incompressible solvers, we do not discretize the diffusion terms using Crank-Nicholson. This is done for two reasons: first of all, because it involves the velocity rather than the momentum and thus it is a nonlinear function of the conservative variables if this term is calculated fully implicitly, which would require iterations. More importantly, if treated implicitly this term will appear in the elliptic equation (3.6) for the updated density and thus disallows the application of the fast spectral solver for the updated density and pressure. Furthermore, for high Reynolds number flow, where $\mathrm{Re}\gg 1$, an explicit diffusion term is clearly adequate [10].

3.4 The L^2 stability

To check the stability, we write the method as a semi-implicit method

$$\frac{U^{n+1}-U^n}{\Delta t}+AU^n+BU^{n+1}=0.$$

We have the following Lemma

Lemma 3.1. *If both methods*

$$\frac{U^{n+1}-U^n}{\Delta t}+AU^n=0,\qquad \frac{U^{n+1}-U^n}{\Delta t}+BU^{n+1}=0$$

are stable, then the original method is also stable.

Proof. Method $U^{n+1}=(I-\Delta tA)U^n$ is stable *iff*

$$\|I-\Delta tA\|\leq 1+c_1\Delta t.$$

Method $U^{n+1}=(I+\Delta tB)^{-1}U^n$ is stable *iff*

$$\|(I+\Delta tB)^{-1}\|\leq 1+c_2\Delta t.$$

Thus the combined method $U^{n+1}=(I+\Delta tB)^{-1}(I-\Delta tA)U^n$ is stable *iff*

$$\|(I+\Delta tB)^{-1}(I-\Delta tA)\|\leq\|(I+\Delta tB)^{-1}\|\|(I-\Delta tA)\|\leq 1+C\Delta t.$$

Therefore, so long as the fast and slow systems are *individually* stable, the combined scheme will also be stable. □

3.5 Spatial discretization of the split systems

For simplicity, assume a uniform grid with spacing Δx and define $\phi_{ij}=\phi(x_i,y_j)$ for any variable ϕ, where $(x_i,y_j)=(\Delta x/2+i\Delta x,\Delta x/2+j\Delta x)$. We also assume for ease of explanation a rectangular domain.

The fast system (3.3) is discretized in space using central differences:

$$\nabla\cdot(\rho\mathbf{u})^{n+1}_{i,j}=D^x_0(\rho u)^{n+1}_{i,j}+D^y_0(\rho v)^{n+1}_{i,j}, \tag{3.7a}$$

$$\frac{a^n}{\varepsilon^2}\nabla\rho^{n+1}_{i,j}=\frac{a^n}{\varepsilon^2}\nabla_0\rho^{n+1}_{i,j}. \tag{3.7b}$$

Here

$$D^x_0\phi_{i,j}=\frac{\phi_{i+1,j}-\phi_{i-1,j}}{2\Delta x},\qquad D^y_0\phi=\frac{\phi_{i,j+1}-\phi_{i,j-1}}{2\Delta x}$$

are the central difference operators,

$$\nabla_0\phi_{i,j}=\begin{pmatrix} D^x_0\phi_{i,j}\\ D^y_0\phi_{i,j}\end{pmatrix}$$

is the natural extension to the central difference gradient and a^n is the value of $a(t)=\min p'(\rho)$ at time $t=t^n$.

We discretize the convective flux terms in (3.2) using a second order central scheme [25], which is a higher-order extension of the Lax-Friedrichs scheme. This choice is by no means unique–any standard shock-capturing scheme will be sufficient. We take the conservative discretization,

$$\mathcal{F}(U^n_{i,j})=\frac{H^n_{i+\frac12,j}-H^n_{i-\frac12,j}}{\Delta x}+\frac{H^n_{i,j+\frac12}-H^n_{i,j-\frac12}}{\Delta x}, \tag{3.8}$$

where

$$H^n_{i+\frac12,j}=\frac12\Big(f(U^n_{i+\frac12,j,+})+f(U^n_{i+\frac12,j,-})-\lambda^n_{i+\frac12,j}(U^n_{i+\frac12,j,+}-U^n_{i+\frac12,j,-})\Big), \tag{3.9a}$$

$$\lambda^n_{i+\frac12,j}=\max\Big\{\sigma\Big(\frac{\partial F}{\partial U}(U_{i+\frac12,j,+})\Big),\sigma\Big(\frac{\partial F}{\partial U}(U_{i+\frac12,j,-})\Big)\Big\}. \tag{3.9b}$$

σ is the spectral radius of the Jacobians in (3.9b), i.e., the maximum wave speed. Here f is the relevant flux function from the slow system (3.2) chosen for x and y fluxes as needed. The edge values $U_{i\pm1/2,j}$ at each interface are reconstructed component-wise using the generalized minmod limiter, with $\theta\in[1,2]$,

$$\sigma^n_j=\text{minmod}\Big(\theta\frac{u^n_{i+1,j}-u^n_{i,j}}{\Delta x},\theta\frac{u^n_{i,j}-u^n_{i-1,j}}{\Delta x},\frac{u^n_{i+1,j}-u^n_{i-1,j}}{2\Delta x}\Big), \tag{3.10a}$$

$$u^n_{i+\frac12,j,+}=u^n_{i+1,j}-\frac{\Delta x}{2}\sigma^n_{i+1,j},\qquad u^n_{i+\frac12,j,-}=u^n_{i,j}+\frac{\Delta x}{2}\sigma^n_{i,j}. \tag{3.10b}$$

Note here that in central schemes, the slope limiter is based on conserved variables rather than a local characteristic decomposition.

The CFL condition for this scheme is, at first order, following [25]

$$\frac{\lambda\Delta t}{\Delta x}\leq\frac{1}{4d}, \tag{3.11}$$

where d is the dimension of the computation and for the second order Adams-Bashforth-Crank-Nicolson scheme it is

$$\frac{\lambda\Delta t}{\Delta x}\leq\frac{1}{2}\frac{1}{8d}. \tag{3.12}$$

The 4 and 8 in the formula are from the number of terms evaluated in the numerical flux in each direction. λ is the sum of the maximum wave speeds in each direction. While this CFL constant is restrictive, it is important to notice that it is independent of ε. In fact, as we will see below from the numerical results, the method performs best in the low Mach number limit when we take $\alpha=\mathcal{O}(\varepsilon^2)$. In this case the wave speeds λ are given by $\lambda=\mathcal{O}(|u|)$ and we have the hyperbolic CFL condition

$$\Delta t\leq\frac{1}{32}\max|u|\Delta x. \tag{3.13}$$

3.6 Boundary and initial conditions

Our example boundary conditions listed in Section 2 only gave the boundary conditions for $\mathbf{u}$, not ρ. To remedy this, we artificially enforce a boundary condition of $\partial\rho/\partial n=0$ on $\partial\Omega$. In the following analysis we will also assume a solid wall boundary with $\mathbf{u}\cdot n=0$ on $\partial\Omega$. For the Navier-Stokes case, we extend this to the no-slip boundary condition $u=0$ on $\partial\Omega$.

We enforce these boundary conditions by using ghost cells, setting

$$\rho_{-1}=\rho_0,\qquad \mathbf{u}_{-1}=-\mathbf{u}_0,\qquad (\rho\mathbf{u})_{-1}=-(\rho\mathbf{u})_0. \tag{3.14}$$

This results in a second order approximation of the boundary condition.

We only consider initial data of the form

$$\rho(0,\mathbf{x})=\rho_0+\varepsilon^2\rho^{(2)}(x)+\cdots, \tag{3.15a}$$
$$\nabla\cdot\mathbf{u}(0,x)=\mathcal{O}(\varepsilon). \tag{3.15b}$$

This initial data converges to admissible initial data of the limiting incompressible equation.

One thing to note is that this is *not* a projection scheme for general initial data. In fact, general initial data will implicitly contain $\mathcal{O}(1/\varepsilon)$ acoustic waves that require resolution in space and time for accuracy and stability. This situation could reflect a poor choice of terms in nondimensionalization, as the behavior of the solution is compressible, not

incompressible. However, in certain cases, such as when the Mach number is not excessively small, the scheme could offer some speedup over a standard solver in that it can take much larger timesteps due to the fact that the acoustic wave term is treated implicitly and the explicit solver only needs to advance the remaining part of the waves.

3.7 The discrete low Mach number limit

Next, we show that in the limit $\varepsilon \ll 1$ this solver automatically transforms into an incompressible solver. In the following, we will write ∇_0 as the standard centered difference gradient operator and $\widetilde{\nabla}$ as the shock-capturing difference operator from (3.9a).

We write

$$\rho_{i,j}^n = \rho_{i,j}^{n,(0)} + \varepsilon^2 \rho_{i,j}^{n,(2)} + \cdots, \tag{3.16a}$$

$$(\rho \mathbf{u})_{i,j}^n = (\rho \mathbf{u})_{i,j}^{n,(0)} + \varepsilon^2 (\rho \mathbf{u})_{i,j}^{n,(2)} + \cdots, \tag{3.16b}$$

$$p_{i,j}^n = p_{i,j}^{n,(0)} + \varepsilon^2 p_{i,j}^{n,(2)} + \cdots = (\rho_{i,j}^{n,(0)})^\gamma + \varepsilon^2 \gamma ((\rho_{i,j}^{n,(0)})^{\gamma-1} \rho_{i,j}^{n,(2)}) + \cdots. \tag{3.16c}$$

We skip ε^1 in the expansion because there are no $\mathcal{O}(\varepsilon^{-1})$ terms in the discrete equations.

We now look at how the terms balance at each order in ε. For small ε, the $\mathcal{O}(\varepsilon^{-2})$ terms are given by

$$\begin{aligned}
&\frac{a^n}{4\Delta x}(\rho_{i+1,j}^{n+1,(0)} - \rho_{i-1,j}^{n+1,(0)} + \rho_{i+1,j}^{n,(0)} - \rho_{i-1,j}^{n,(0)}) = 0, \\
&\frac{a^n}{4\Delta x}(\rho_{i,j+1}^{n+1,(0)} - \rho_{i,j-1}^{n+1,(0)} + \rho_{i,j+1}^{n,(0)} - \rho_{i,j-1}^{n,(0)}) = 0, \\
\Rightarrow\ & \rho_{i+1,j}^{n+1,(0)} - \rho_{i-1,j}^{n+1,(0)} = -(\rho_{i+1,j}^{n,(0)} - \rho_{i-1,j}^{n,(0)}) = 0, \qquad \rho_{i+1,j}^{n+1,(0)} = \rho_{i-1,j}^{n+1,(0)}, \\
\Rightarrow\ & \rho_{i,j+1}^{n+1,(0)} - \rho_{i,j-1}^{n+1,(0)} = -(\rho_{i,j+1}^{n,(0)} - \rho_{i,j-1}^{n,(0)}) = 0, \qquad \rho_{i,j+1}^{n+1,(0)} = \rho_{i,j-1}^{n+1,(0)}.
\end{aligned}$$

This result comes from the fact that the leading order density was constant at the previous timestep, consistent with the initial condition (3.15).

A straightforward application of the boundary conditions (3.14) gives $\rho_{i,j}^{n+1,(0)} = \rho_0^{n+1}$, $\forall i,j$, a constant in space but not necessarily in time. Next one needs to show incompressibility and this is where the α terms in the splitting become important. The $\mathcal{O}(1)$ equation for the density is given by

$$\begin{aligned}
\frac{\rho_{i,j}^{n+1,(0)} - \rho_{i,j}^{n,(0)}}{\Delta t} &+ \alpha \widetilde{\nabla}_0 \Big(\frac{3}{2}(\rho \mathbf{u}^n) - \frac{1}{2}(\rho \mathbf{u})^{n-1} \Big) \\
&+ \frac{1-\alpha}{2} \Big(\nabla_0 \cdot (\rho_{i,j}^{n+1,(0)} \mathbf{u}_{i,j}^{n+1,(0)}) + \nabla_0 (\rho_{i,j}^{n+1,(0)} \mathbf{u}_{i,j}^{n,(0)}) \Big) = 0.
\end{aligned}$$

Note that $\widetilde{\nabla}$ reduces to ∇_0 in this case, as the density jump at the interface is zero due to the constant profile of $\rho^{(0)}$, resulting in a numerical dissipation term of $\lambda_{i+1/2,j}^n (\rho_{i+1/2,j,+}^{(0),n} -$

$\rho^{(0),n}_{i+1/2,j,-}))$ (note that the dissipation would not be of this form if a slope limiter based on a local characteristic decomposition is used).

We now do the discrete analog of the integrals done in Section 2.1 by summing this equation over all i, j. Recalling that the leading order density is a constant and noting that the flux terms telescope and the resulting boundary terms cancel out, these result in

$$N^2\rho_0^{n+1}-\sum_{i,j}\rho_{i,j}^{n,(0)}=0 \quad \Rightarrow \quad \rho_0^{n+1}=\frac{1}{N}\sum_{i,j}\rho_{i,j}^{n,(0)}, \tag{3.17}$$

where N is the total number of grid points in each direction. This merely says that the new density is a constant and is simply equal to the average value of the density at the previous time step. Furthermore, as the density in the previous time step was also constant to leading order in space this says that the two coincide, so the density is also constant in time as was seen in the continuous case.

Using this result, the density terms cancel out and we are left with

$$\frac{3}{2}\alpha\nabla_0\cdot(\rho^{(0)}\mathbf{u}^{(0)})^n-\frac{1}{2}\alpha\nabla_0\cdot(\rho^{(0)}\mathbf{u}^{(0)})^n+(1-\alpha)\rho^{n+1,(0)}\frac{1}{2}(\nabla_0\cdot(\mathbf{u}^{n+1,(0)}+\mathbf{u}^{n,(0)}))=0.$$

As we assumed the initial velocity field was incompressible to $\mathcal{O}(\varepsilon)$, the terms from the t^n step drop out and we are left with $\nabla_0\cdot\mathbf{u}^{n+1,(0)}=0$, the discrete incompressibility condition for $\mathbf{u}^{n+1,(0)}$.

Finally, we can derive an equation for the density correction term $\rho^{n+1,(2)}$ (and hence the incompressible pressure $p^{(2)}$) by looking at the $\mathcal{O}(1)$ terms in the elliptic equation reformulation (3.6)

$$\begin{aligned}
&\frac{\rho^{n+1,(0)}-\rho^{n,(0)}}{\Delta t}+\alpha\nabla_0\cdot\Big(\frac{3}{2}(\rho\mathbf{u})^{n,(0)}-\frac{1}{2}(\rho\mathbf{u})^{n-1,(0)}\Big)+(1-\alpha)\Delta t\nabla_0\cdot(\rho\mathbf{u})^{n,(0)}\\
&\quad-\frac{(1-\alpha)\Delta t}{2}\nabla_0\cdot\widetilde{\nabla}\cdot\Big(\frac{3}{2}(\rho\mathbf{u}\otimes\mathbf{u})^{n,(0)}-\frac{1}{2}(\rho\mathbf{u}\otimes\mathbf{u})^{n-1,(0)}\Big)\\
&\quad-\frac{(1-\alpha)\Delta t}{2}\nabla_0\cdot\widetilde{\nabla}\Big(\frac{3}{2}\Big(\frac{p(\rho)-a^n\rho}{\varepsilon^2}\Big)^{n,(0)}-\frac{1}{2}\Big(\frac{p(\rho)-a^n\rho}{\varepsilon}\Big)^{n-1,(0)}\Big)\\
&\quad-\frac{(1-\alpha)a^n\Delta t}{2}\nabla_0\cdot\nabla_0\frac{\rho^{n+1,(2)}+\rho^{n,(2)}}{2}=\frac{1}{\mathrm{Re}}\frac{(1-\alpha)\Delta t}{2}\nabla_0\cdot\Delta\Big(\frac{3}{2}\mathbf{u}^{n,(0)}-\frac{1}{2}\mathbf{u}^{n-1,(0)}\Big).
\end{aligned} \tag{3.18}$$

Again, we have used the fact that $\widetilde{\nabla}=\nabla_0$ for the explicit flux terms in the leading order density equation. We can rewrite this as

$$-\frac{a^n}{4\Delta x^2}(\rho_{i+2,j}^{n+1,(2)}+\rho_{i-2,j}^{n+1,(2)}+\rho_{i,j+2}^{n+1,(2)}+\rho_{i,j-2}^{n+1,(2)}-4\rho_{i,j}^{n+1,(2)})=\phi(U^{n,(0)},U^{n+1,(0)}),$$

where ϕ collects all the explicit or known terms. This is simply a Poisson equation for $\rho^{n+1,(2)}$. Using the expansion of the pressure (3.16c) and the definition of a^n, one has that

$a^n\rho^{(2)}=p^{(2)}$. Using this fact and the knowledge of the previous steps' leading order density and incompressibility one obtains a discretization of the pressure Poisson equation

$$-\Delta_2 p^{(2)} = -\nabla_0\cdot\widetilde{\nabla}\cdot\Big(\frac{3}{2}(\rho\mathbf{u}\otimes\mathbf{u})^{n,(0)}-\frac{1}{2}(\rho\mathbf{u}\otimes\mathbf{u})^{n-1,(0)}\Big) + \frac{1}{\mathrm{Re}}\nabla_0\cdot\Delta_0\Big(\frac{3}{2}\mathbf{u}^{n,(0)}+\frac{1}{2}\mathbf{u}^{n-1,(0)}\Big). \tag{3.19}$$

Here, Δ_0 is the standard centered second order Laplacian and Δ_2 is the second order centered Laplacian with stencil of size $4\Delta x$ generated by $\nabla_0\cdot\nabla_0$. In the continuous case, the divergence and Laplacian would commute and the diffusion-type term would drop out due to incompressibility, but this is not necessarily true at the discrete level. We also note that the explicit pressure term drops out, as the modified explicit pressure $\varepsilon^{-2}(p(\rho)-a(t)\rho)$ has a simple Taylor expansion for small ε of

$$\widetilde{p}_\varepsilon=\frac{1}{\varepsilon^2}\big((\rho_0)^\gamma+\gamma\varepsilon^2(\rho_0)^{\gamma-1}\rho_{i,j}^{n+1,(2)}-a^n(\rho_0+\varepsilon^2\rho_{i,j}^{n+1,(2)})\big).$$

For convex equations of state (such as the one we are using), a^n is found at $\rho_{\min}:=\rho^\dagger$, which will not deviate much from ρ_0. Thus we have

$$a^n:=p'(\rho^\dagger)=\gamma\rho_0^{\gamma-1}+\gamma(\gamma-1)\varepsilon^2\rho_0^{\gamma-2}(\rho^\dagger-\rho_0)=\gamma\rho_0^{\gamma-1}+\mathcal{O}(\varepsilon^4),$$

as $\rho^\dagger-\rho=\mathcal{O}(\varepsilon^2)$. Therefore,

$$\frac{1}{\varepsilon^2}\big((\rho_0)^\gamma+\gamma\varepsilon^2(\rho_0)^{\gamma-1}\rho_{i,j}^{n+1,(2)}-a^n(\rho_0+\varepsilon^2\rho_{i,j}^{n+1,(2)})\big)=\frac{1}{\varepsilon^2}(1-\gamma)\rho_0^{\gamma-1}.$$

Thus the explicit pressure becomes a constant in the low Mach number limit. In principle, one can also subtract a constant derived from the density (such as the average or minimum density) to ensure that this constant background pressure does not become too large, but in practice it does not really matter because this pressure term is only seen as a derivative, so the background constant value does not matter. Thus we have found that, to $\mathcal{O}(1)$, the modified pressure in the slow system (3.2) becomes constant in space in the low Mach number limit.

For the momentum equations, at $\mathcal{O}(1)$

$$\frac{\mathbf{u}_{i,j}^{n+1,(0)}-\mathbf{u}_{i,j}^{n,(0)}}{\Delta t}+\widetilde{\nabla}\Big(\frac{3}{2}\mathbf{u}_{i,j}^{n,(0)}\otimes\mathbf{u}_{i,j}^{n,(0)}-\frac{1}{2}\mathbf{u}_{i,j}^{n-1,(0)}\otimes\mathbf{u}_{i,j}^{n-1,(0)}\Big) + \nabla_0\frac{1}{2}(p_{i,j}^{n+1,(2)}+p_{i,j}^{n,(2)})=\frac{1}{\mathrm{Re}}\Delta_0\Big(\frac{3}{2}\mathbf{u}_{i,j}^{n,(0)}-\frac{1}{2}\mathbf{u}_{i,j}^{n,(0)}\Big).$$

This is an equivalent (conservative) formulation of the incompressible momentum equation.

Remark 3.1. When the second-order formulation (3.4a)-(3.4b) is used, the implicit terms contribute no numerical dissipation to the system, i.e., the only numerical dissipation is the $\mathcal{O}(1)$ contribution from the explicit, slow flux terms. We sketch the proof of this in one dimension; the proof for higher dimensions is similar.

The terms of the semi-implicit formulation from the fast system are

$$\frac{\rho_j^{n+1}-\rho_j^n}{\Delta t}+(1-\alpha)\frac{1}{2}\Big(\frac{(\rho u)_{j+1}^{n+1}-(\rho u)_{j-1}^{n+1}}{\Delta x}+\frac{(\rho u)_{j+1}^{n}-(\rho u)_{j-1}^{n}}{\Delta x}\Big)=0, \tag{3.20a}$$

$$\frac{(\rho u)_j^{n+1}-(\rho u)_j^n}{\Delta t}+\frac{a}{\varepsilon^2}\frac{1}{2}\Big(\frac{\rho_{j+1}^{n+1}-\rho_{j-1}^{n+1}}{\Delta x}+\frac{\rho_{j+1}^{n}-\rho_{j-1}^{n}}{\Delta x}\Big)=0. \tag{3.20b}$$

Note that for $\varepsilon\ll 1$ one can assume that a is constant to leading order. One needs to make sure that numerical dissipation does not dominate when ε is small.

Define the discrete energy functional

$$\mathcal{L}^{n+1}=\sum_{j=1}^{N}\Big(\frac{\rho^{n+1}-\rho^n}{\Delta t}\Big)^2+\frac{(1-\alpha)a}{\varepsilon^2}\Big(\frac{1}{2}\Big(\frac{\rho_{j+1}^{n+1}-\rho_{j-1}^{n+1}}{2\Delta x}\Big)+\Big(\frac{\rho_{j+1}^{n}-\rho_{j-1}^{n}}{2\Delta x}\Big)\Big)^2.$$

By taking the time difference of (3.20a) and the divergence of (3.20b), summing over the domain and using summation by parts, one can derive that

$$\mathcal{L}^{n+1}-\mathcal{L}^n=0,$$

which implies that the implicit terms introduce no numerical dissipation into the solution.

In summary, the limiting incompressible scheme is

$$\rho_{i,j}^{(0)}=\rho_0, \tag{3.21a}$$

$$\nabla_0\cdot\mathbf{u}_{i,j}^{n+1,(0)}=0, \tag{3.21b}$$

$$\begin{aligned}-\Delta_2 p^{n+1,(2)}=&-\nabla_0\cdot\widetilde{\nabla}\cdot\Big(\frac{3}{2}(\rho\mathbf{u}\otimes\mathbf{u})^{n,(0)}-\frac{1}{2}(\rho\mathbf{u}\otimes\mathbf{u})^{n-1,(0)}\Big)\\&+\frac{1}{\mathrm{Re}}\nabla_0\cdot\Delta_0\Big(\frac{3}{2}\mathbf{u}^{n,(0)}+\frac{1}{2}\mathbf{u}^{n-1,(0)}\Big),\end{aligned} \tag{3.21c}$$

$$\begin{aligned}&\frac{\mathbf{u}_{i,j}^{n+1,(0)}-\mathbf{u}_{i,j}^{n,(0)}}{\Delta t}+\widetilde{\nabla}\Big(\frac{3}{2}\mathbf{u}_{i,j}^{n,(0)}\otimes\mathbf{u}_{i,j}^{n,(0)}-\frac{1}{2}\mathbf{u}_{i,j}^{n-1,(0)}\otimes\mathbf{u}_{i,j}^{n-1,(0)}\Big)\\&\quad+\nabla_0\frac{1}{2}(p_{i,j}^{n+1,(2)}+p_{i,j}^{n,(2)})=\frac{1}{\mathrm{Re}}\Delta_0\Big(\frac{3}{2}\mathbf{u}_{i,j}^{n,(0)}-\frac{1}{2}\mathbf{u}_{i,j}^{n,(0)}\Big).\end{aligned} \tag{3.21d}$$

This is a second order version of a projection type method [3, 30].

3.8 The fast solver for ρ^{n+1}

One can efficiently solve the elliptic equation (3.6) using fast Fourier transform (FFT) based solvers. Here we will sketch the basic idea for the homogeneous Neumann boundary conditions; for further details on the development of these methods see Swarztrauber [29] and for further information on using FFT techniques on different gridding systems and boundary conditions, see Bradford [2].

The basic idea is to expand the solution in trigometric functions that are consistent with the boundary conditions. The expansion derived below is for a cell-centered grid with the homogeneous Neumann boundary conditions, but it is relatively straightforward to find an expansion for other typical boundary conditions. For a system with N grid points placed at $x_{i+1/2,j+1/2}=(\Delta x/2+i/N,\Delta x/2+j/N)$ on $(0,1)\times(0,1)$ and homogeneous Neumann boundary conditions for ρ, we expand using $\cos(\pi k(j+1/2)/N)$, $k=0,\cdots,N-1$. Therefore, we assume

$$\rho_{i,j}^{n+1}=\sum_{k=0}^{N-1}\hat{\rho}_{k,j}\cos(\pi k(i+1/2)/N).$$

Sticking this into the elliptic equation (3.6) for ρ^{n+1} and using the orthogonality of the basis functions give

$$\hat{\rho}_{k,j}\Big(1+4\frac{(1-\alpha)a\Delta t^2}{16\varepsilon^2\Delta x^2}\sin^2\Big(\frac{\pi k}{N}\Big)\Big)-\frac{(1-\alpha)a\Delta t^2}{16\varepsilon^2\Delta x^2}(\hat{\rho}_{k,j+2}+\hat{\rho}_{k,j-1})=\hat{\phi}_{k,j}.$$

Here, $\hat{\phi}_{k,j}$ is the transformed right-hand side in the expansion functions chosen. This gives a tridiagonal system for solving $\hat{\rho}_{k,j}$, which is then transformed back onto the grid. Determination of the coefficients $\hat{\phi}_{k,j}$ is done through the use of the staggered Fourier transforms [2], as is the inverse transform back to the physical grid. The boundary conditions are automatically built into this framework by the choice of the basis function.

In two dimensions, this transform only needs to be done along one space dimension. The resulting system will be tridiagonal and can thus be solved in $\mathcal{O}(N)$ steps. Therefore, the overall computational cost is $\mathcal{O}(N\log N)$.

4 Numerical results

4.1 Compressible flow examples ($\varepsilon=\mathcal{O}(1)$)

Experimentation with the artificial splitting parameter α in compressible regimes (i.e., $\varepsilon=\mathcal{O}(1)$) showed that there is little effect on the solution unless α is chosen close to 0. In the compressible examples below, we show results for $\alpha=0.5$. The timestep is chosen according to the CFL condition (3.12).

1D Riemann problem. First, we will demonstrate the method in a compressible regime, i.e., where the Mach number is $\mathcal{O}(1)$. We start with a 1-d Riemann problem with the

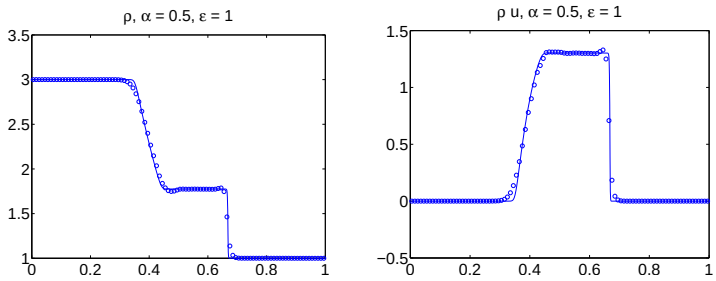

(a) ρ, $\alpha=0.5$ (b) ρu, $\alpha=0.5$

Figure 1: 1D Riemann problem with initial data (4.1). $\varepsilon=1$, $\gamma=1.4$, $\alpha=0.5$. The solid line is the true solution.

initial condition

$$\rho(x,0)=\begin{cases} 3.0, & x<1/2, \\ 1.0, & x\geq 1/2, \end{cases} \qquad u(x,0)=0. \tag{4.1}$$

We discretize this problem with 100 points and choose $\varepsilon=1$, $\gamma=1.4$ and $\theta=1$ (the minmod slope limiter) for a spatially second order scheme. The results are found in Fig. 1. The scheme captures the correct shock speed. The overshoots in the result are an artifact of the central scheme used for the numerical fluxes and diminish as the grid is refined.

Higher Mach number. Next we test the performance of the scheme at a higher Mach number. We take the same setup and parameters as in the previous Sod problem (1), but now set $\varepsilon=20$. The results are found in Fig. 2.

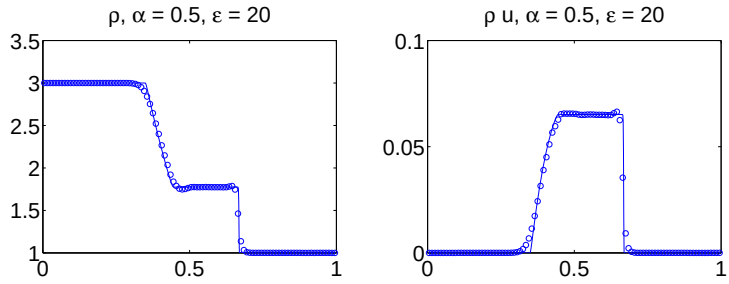

(a) ρ, $\alpha=0.5$ (b) ρu, $\alpha=0.5$

Figure 2: 1D Riemann problem with initial data (4.1). $\varepsilon=20$, $\gamma=1.4$, $\alpha=0.5$. The solid line is the true solution.

Strong shock wave. Next, we test a strong shock to check that the scheme captures the correct wave speed. Inspired by the example from [21], we take the initial data

$$\rho(x,0)=\begin{cases} 10.0, & x<1/2, \\ 20.0, & x\geq 1/2, \end{cases} \qquad u(x,0)=\begin{cases} 2000.0, & x<1/2, \\ 0.0, & x\geq 1/2. \end{cases} \tag{4.2}$$

We use 500 points and set $\varepsilon=1$, $\gamma=1.4$, $\theta=1$. The results are given in Fig. 3. Again, the scheme appears to be able to capture the correct shock speed, though the strength of

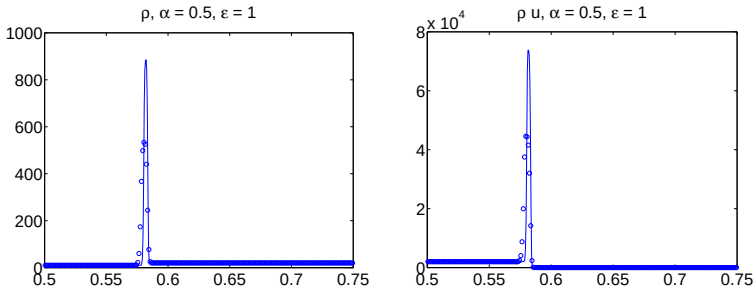

(a) ρ (b) ρu

Figure 3: Solution to initial data (4.2) at $T=0.001$ with $\varepsilon=1$ and $\alpha=0.5$. The solid line is the true solution.

the shock demands a large amount of numerical diffusion which smears the peak of the strong shock.

2D Riemann problem. We also run a test on a 2D Riemann problem inspired by the initial data in [27] for the full Euler equations. Here we set $\varepsilon=1$, $\gamma=1.4$ and choose the initial data as

$$\rho(x,y,0)=\begin{cases} 0.5323, & x<1/2,\ y\geq 1/2, \\ 0.138, & x<1/2,\ y<1/2, \end{cases} \quad \begin{cases} 1.5, & x\geq 1/2,\ y\geq 1/2, \\ 0.5323, & x\geq 1/2,\ y<1/2, \end{cases} \tag{4.3a}$$

$$u(x,y,0)=\begin{cases} 1.206, & x<1/2,\ y\geq 0, \\ 1.206, & x<1/2,\ y<1/2, \end{cases} \quad \begin{cases} 0, & x\geq 1/2,\ y\geq 1/2, \\ 0, & x\geq 1/2,\ y<1/2, \end{cases} \tag{4.3b}$$

$$v(x,y,0)=\begin{cases} 0, & x<1/2,\ y\geq 0, \\ 1.206, & x<1/2,\ y<1/2, \end{cases} \quad \begin{cases} 0, & x\geq 1/2,\ y\geq 1/2, \\ 1.206, & x\geq 1/2,\ y<1/2. \end{cases} \tag{4.3c}$$

This initial data results in four shock waves. As in the 1D case and we take 50 points in each direction. The results are given in Fig. 4.

4.2 Low Mach number limit examples $(\varepsilon \ll 1)$

In all of the examples below, the numerical experimentation has revealed that choosing $\alpha=\varepsilon^2$ provides good results in small ε regimes. The timesteps are chosen according to the CFL condition (3.13).

Periodic flow. First, we test a simple problem with periodic boundary conditions, to divorce the AP property from any boundary peculiarities. This example was used in [8]. The initial conditions and constant γ are

$$\begin{cases} \rho(0,x,y)=1+\varepsilon^2\sin^2(2\pi(x+y)), \\ u(0,x,y)=\sin(2\pi(x-y)), \\ v(0,x,y)=\sin(2\pi(x-y)), \\ \gamma=2. \end{cases} \tag{4.4}$$

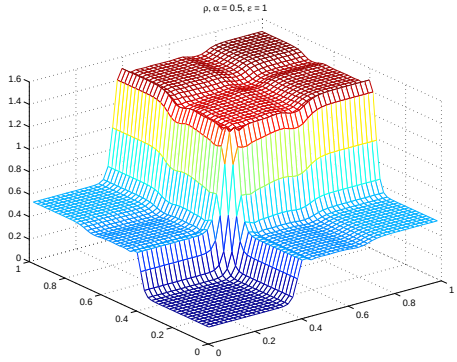

Figure 4: Density plot of 2D Riemann problem with initial data (4.3). $\varepsilon=1$, $\gamma=1.4$, $\alpha=0.5$.

The initial velocity field is divergence free and the density field is constant at leading order. We fix the Reynolds number at $\mathrm{Re}=100$, the spatial step at $\Delta x=1/32$ and the temporal step at 2.5×10^{-4} and look at ε values of 0.1 and 10^{-4}. Figs. 5-6 compare the solution given by the AP scheme at $T=1$ to a highly resolved solution. In both cases we see that there is little error between the two, especially in the $\varepsilon=10^{-4}$ case, where Δx

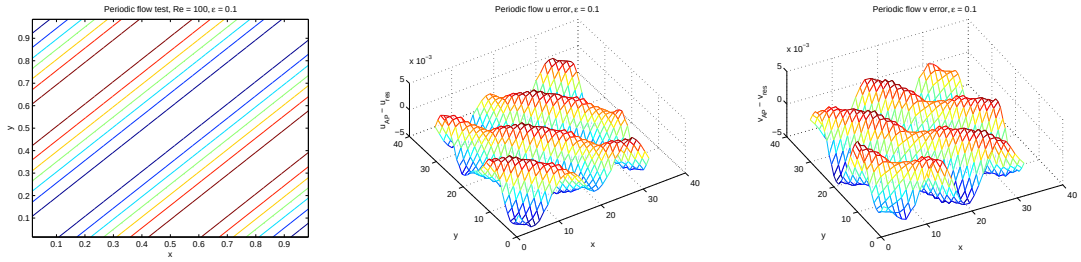

(a) $\varepsilon=0.1$. (b) $\varepsilon=0.1$. (c) $\varepsilon=0.1$.

Figure 5: Results for periodic flow test case (4.4), $\varepsilon=0.1$. (a): stream function of solution with $\Delta x=1/16$. (b): error in u. (c): error in v.

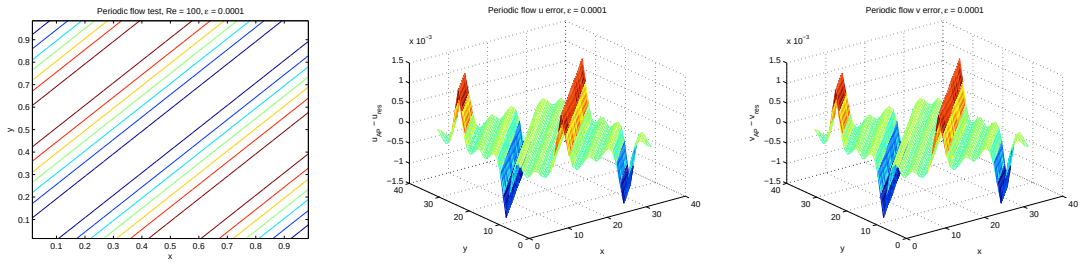

(a) $\varepsilon=0.0001$. (b) $\varepsilon=0.0001$. (c) $\varepsilon=0.0001$.

Figure 6: Results for periodic flow test case (4.4), $\varepsilon=10^{-4}$. (a): stream function of solution with $\Delta x=1/16$. (b): error in u. (c): error in v.

grossly underresolves ε. As Δx and Δt become small, the $\mathcal{O}(\varepsilon)$ model error dominates the error, as expected.

Vortex-in-a-box. Next, we test a similar case that was used in [5]. This is the so-called "vortex in a box", given by

$$\begin{cases} \rho(0,x,y)=1-\frac{\varepsilon^2}{2}\tanh(y-1/2), \\ u(0,x,y)=2\sin^2(\pi x)\sin(\pi y)\cos(\pi y), \\ v(0,x,y)=-2\sin(\pi x)\cos(\pi x)\sin^2(y), \\ \gamma=1.4. \end{cases} \tag{4.5}$$

The boundary condition is now a no-slip boundary condition ($\mathbf{u}=0$ on $\partial\Omega$). We again fix the Reynolds number at $\mathrm{Re}=100$, the spatial step at $\Delta x=1/64$ and the temporal step at 2.5×10^{-4} and drive ε to zero. The solution at $T=0.125$ using the AP scheme is compared to a highly resolved solution in Figs. 7-8. As in the previous case, when Δx and Δt become small the $\mathcal{O}(\varepsilon)$ model error dominates the error, as expected.

Backward facing step flow. Next, we test a problem with non-zero velocity boundary conditions. We examine the case of flow over a backward facing step, as found in [28]. The computational domain for this problem is $\Omega=[0,L]\times[-0.5,0.5]$. A no-flow boundary condition $(u,v)\cdot\hat{n}=0$ is given for the step ($x=0$, $-0.5\leq y\leq 0$) and the top and bottom walls. The velocity in the left, inflow boundary is given by $(u,v)=(12y(1-2y),0)$ on ($x=0$, $0\leq y\leq 0.5$) and the outflow velocity is given as $(u,v)=(-3y^2+3/4,0)$, ($x=L$, $-0.5\leq y\leq 0.5$) These boundary conditions are slowly ramped up from time 0 to time 1 by the function $0.5(1-\cos(\pi t))$. A Neumann boundary condition for the density (and thus the pressure) is enforced on all of the boundaries.

In Fig. 9, we compare the AP scheme solution for $\varepsilon=0.01$ and a Reynolds number of 100 with the incompressible solution computed by Liu et al. in [28]. We take $\Delta x=1/16$, $\Delta t=9.765\times10^{-4}$ and a channel of length $L=8$.

In comparing the solution in Fig. 9, we see that the reattachment point of the circulation region behind the step matches with the results found in [28].

4.3 Rate of convergence test

Here we verify the temporal and spatial order of accuracy of the scheme in compressible regimes as well as the low Mach number limit.

$\varepsilon=\mathcal{O}(1)$ test. First we verify the order of convergence away from the low Mach number regime by setting $\varepsilon=1$. We take a domain of $\Omega=[0,1]\times[0,1]$ with $\mathbf{u}=0$ on $\partial\Omega$ and a symmetric initial condition of

$$\begin{cases} \rho=1+0.5e^{-100((x-1/2)^2+(y-1/2)^2)}, \\ u=0, \\ v=0. \end{cases} \tag{4.6}$$

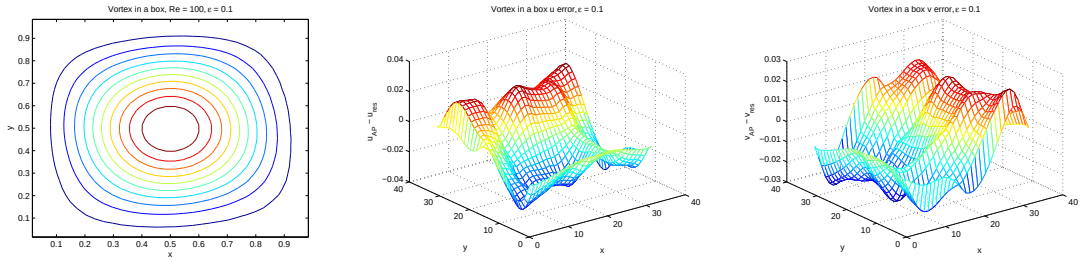

(a) Stream function $\varepsilon=0.1$. (b) u error, $\varepsilon=0.1$. (c) v error, $\varepsilon=0.1$.

Figure 7: Results for vortex in a box flow (4.5) at $T=0.125$, $\varepsilon=0.1$. (a): stream function of solution with $\Delta x=1/16$. (b): error in u. (c): error in v.

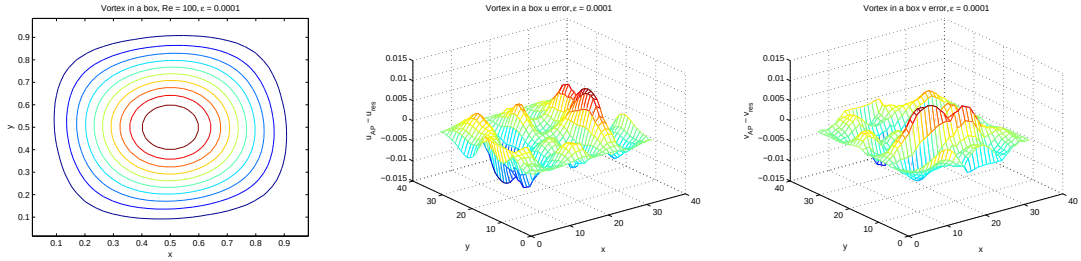

(a) Stream function $\varepsilon=0.0001$. (b) u error, $\varepsilon=0.0001$. (c) v error, $\varepsilon=0.0001$.

Figure 8: Results for vortex in a box flow (4.5) at $T=0.125$,$\varepsilon=10^{-4}$. (a): stream function of solution with $\Delta x=1/16$. (b): error in u. (c): error in v.

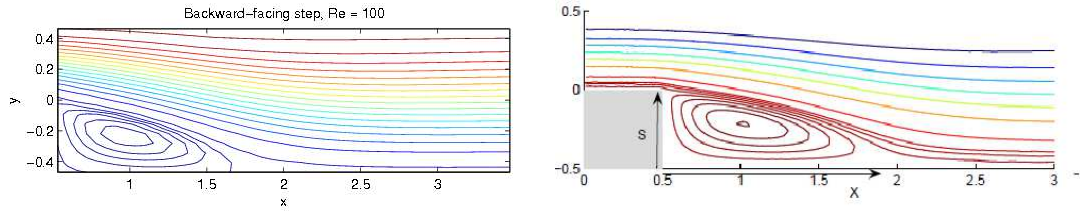

Figure 9: Left: Contour plot of streamfunction for backwards step flow with $\varepsilon=0.01$, $\Delta x=1/N=1/16=0.0625$, $\Delta t=9.765\times10^{-4}$, Re$=100$, $\gamma=1.4$, $\alpha=\varepsilon^2$ and $\theta=1$ at $T=20$. Right: Contour plot of streamfunction from [28]. The AP scheme captures the reattachment point of the circulation region.

To verify the order, we begin with $\Delta x=1/16$ and $\Delta t=0.0018$ (based on the CFL condition (3.13)) and refine the simulation dyadically, fixing the ratio $\Delta t/\Delta x=0.288$ for all simulations. We use $\alpha=0.5$, $Re=100$ and run the simulation to the final time $t=0.01$. A finely resolved 1024×1024 computation is used for the reference solution. The results are listed in Fig. 10. Only the horizontal component ρu is listed, as due to the symmetry of the problem the vertical velocity terms have the same values. The results show second-order convergence, as expected.

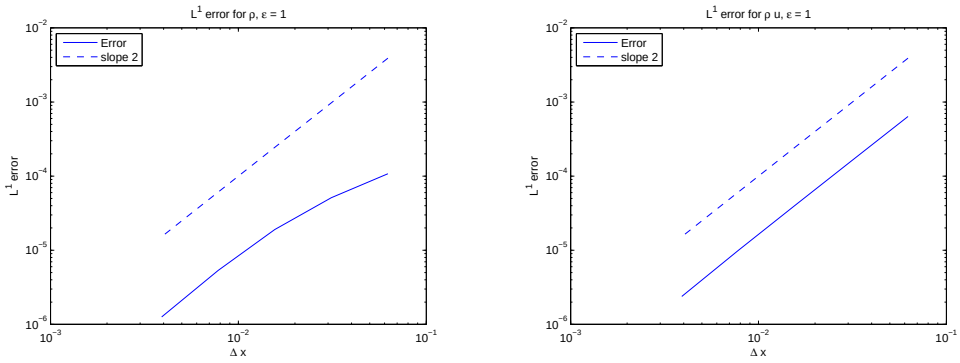

Figure 10: Convergence for Vortex in a box example with $\varepsilon=1$. Left: ρ. Right: ρu. The system is computed to time $t=0.01$ with $\alpha=0.5$, $Re=100$. Solid line: L^1 error of computed solution against a highly resolved reference solution. Dashed line: line with slope 2 for convergence rate comparison.

$\varepsilon \ll 1$ **test.** For the low Mach number regime, we use the vortex-in-a-box initial condition (4.5) with solid walls and $\varepsilon=10^{-4}$, $\alpha=\varepsilon^2$ and $Re=100$. As in the test case above, we begin with $\Delta x=1/16$ and $\Delta t=4.30\times10^{-4}$ (computed from the CFL condition (3.13)), fixing the ratio $\Delta t/\Delta x$ for all simulations. We run the simulation to the final time $t=0.01$. The results are listed in Fig. 11. Only the horizontal component ρu is listed, as due to the symmetry of the problem the vertical velocity terms have the same values and we exclude the density ρ results as the $\mathcal{O}(\varepsilon^2)$ deviations from unity are so small. The minmod slope limiter (3.10b) is replaced with a central difference to generate the slopes, as the solution is expected to be smooth. Due to the stiffness of the compressible problem, a high-resolution reference solution is too expensive to compute, thus the errors are computed by comparing the solution with the numerical solution generated by $\Delta x/2$, $\Delta t/2$.

The results appear to be converging superlinearly rather than quadratically. We know that for $\varepsilon=\mathcal{O}(1)$ our scheme is second order through simple truncation analysis for hy-

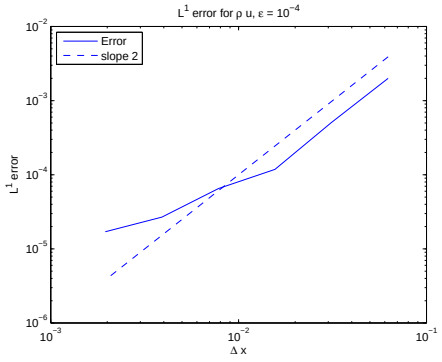

Figure 11: Convergence for Vortex in a box example with $\varepsilon=10^{-4}$. The system is computed to time $t=0.01$, $\alpha=\varepsilon^2$ and $Re=100$. The computed solutions are compared to the solution with the next mesh $(\Delta x/2,\Delta t/2)$ as the reference compressible solution is too expensive to compute. Solid line: L^1 error of computed solution. Dashed line: line with slope 2 for convergence rate comparison.

perbolic systems and in the limit our scheme asymptotically becomes a second order projection method, which also has its own error estimate showing that it is second order. However, we do not have an error estimate for the transition regime of small but finite ε, which may be causing this drop in the convergence rate. As shown in [12, 18], the error between the scheme and the compressible equations for any ε is at worst first order.

5 Concluding remarks and future work

We proposed a new numerical method for solution of the compressible isentropic Euler (and Navier-Stokes) equations that is stable and accurate for any Mach number. The method is based on a hyperbolic splitting that splits the compressible Euler equations into a slowly moving nonlinear conservative hyperbolic system and a fast moving stiff linear acoustic system. The slow part is suitable for modern shock capturing methods, while the stiff acoustic system is solved implicitly with a fast Poisson solver as in a typical projection type method for incompressible flows. This scheme allows the use of time step and space mesh size independent of the Mach number. When the Mach number goes to zero it effectively becomes a second order projection type method for incompressible flows, a property called asymptotic-preserving. Numerical results in one and two space dimensions demonstrate that the scheme is adequate in both compressible and incompressible regimes, capturing shocks with a high resolution in the compressible regime and the incompressible features for small Mach numbers. We also showed that the scheme can offer some speedup in some cases where the initial data that does not follow the low Mach number limit.

In future work we will extend this approach to the full Euler (and Navier-Stokes) equations. The splitting used here relies heavily on the structure of the equation of state for the isentropic Euler equations. Developing a similar splitting for the full equations is more difficult as the incompressibility condition is enforced through the equation of state rather than the mass conservation equation and maintaining hyperbolicity of the slow portion of the equations is more complicated. The limiting incompressible equations for the full system allow for variable density flows, as opposed to constant density in the isentropic case. This could prove to be an important development in the simulation of two-phase flows such as bubbles in water, mostly incompressible flows with regions of high compressibility such as underwater explosions [20], or atmospheric flows. We will also look to extend this work to adaptive time and spatial stepping to allow it to transition between compressible and incompressible regimes as the situation warrants, such as cases where the fast compressible waves leave the computational domain leaving incompressible conditions in their wake.

Acknowledgments

J.-G. Liu was supported by NSF grant DMS 10-11738. J. Haack and S. Jin were supported by NSF grant DMS-0608720 and the NSF FRG grant "Collaborative research on Kinetic

Description of Multiscale Phenomena: Modeling, Theory and Computation" (NSF DMS-0757285). S. Jin was also supported by a Van Vleck Distinguished Research Prize and a Vilas Associate Award from University of Wisconsin-Madison. J. Haack was also supported by the Center for Nonlinear Studies at Los Alamos National Laboratory for a portion of this work. He thanks C. Hauck, R. Lowrie and everyone at CNLS for their valuable insights and support on this project.

References

[1] S. Abarbanel, P. Duth and D. Gottlieb, Splitting methods for low Mach number Euler and Navier-Stokes equations, Comput. Fluids, 17 (1989), 1–12.
[2] B. Bradford, The fast staggered transform, composite symmetries and compact symmetric algorithms, IBM J. Res. Develop, 38 (1994), 117–129.
[3] A. Chorin, Numerical solution of the Navier-Stokes equations, Math. Comput., 22 (1968), 745–762.
[4] A. Chorin, A numerical method for solving incompressible viscous flow problems, J. Comput. Phys., 2 (1967), 12–26.
[5] P. Colella and K. Pao, A projection method for low speed flows, J. Comput. Phys., 149 (1999), 245–269.
[6] P. Crispel, P. Degond and M.-H. Vignal, An asymptotic preserving scheme for the two-fluid Euler-Poisson model in the quasineutral limit, J. Comput. Phys., 223 (2007), 208–234.
[7] P. Degond, S. Jin and J.-G. Liu, Mach-number uniform asymptotic-preserving gauge schemes for compressible flows, Bulletin of the Institute of Mathematics, Academia Sinica, New Series, 2(4) (2007), 851–892.
[8] P. Degond and M. Tang, All speed scheme for the low Mach number limit of the isentropic Euler equation, Commun. Comput. Phys., 10 (2011), 1–31.
[9] P. Degond, J.-G. Liu and M.-H. Vignal, Analysis of an asymptotic preserving scheme for the Euler-Poisson system in the quasineutral limit, SIAM J. Num. Anal., 46 (2008), 1298–1322.
[10] W. E and J.-G. Liu, Vorticity boundary condition and related issues for finite difference schemes, J. Comput. Phys., 124 (1996), 368–382.
[11] C. Gatti-Bono and P. Colella, An analastic allspeed projection method for gravitationally stratified flows, J. Comput. Phys., 216 (2006), 589–615.
[12] F. Golse, S. Jin and C. D. Levermore, The convergence of numerical transfer schemes in diffusive regimes I: the discrete-ordinate method, SIAM J. Numer. Anal., 36 (1999), 1333–1369.
[13] H. Guillard and C. Viozat, On the behaviour of upwind schemes in the low Mach number limit, Comput. Fluids, 28 (1998), 63–86.
[14] B. Gustaffson and H. Stoor, Navier-Stokes equations for almost incompressible flow, SIAM J. Numer. Anal., 28 (1991), 441–454.
[15] F. H. Harlow and A. Amsden, A numerical fluid dynamics calculation method for all flow speeds, J. Comput. Phys., 8 (1971), 179–213.
[16] F. H. Harlow and J. E. Welch, Numerical calculation of time-dependent viscous incompressible flow of fluid with free surface, Phys. Fluid, 8 (1965), 2182–2189.
[17] S. Jin, Efficient asymptotic-preserving (AP) schemes for some multiscale kinetic equations, SIAM J. Sci. Comput., 21 (1999), 441–454.

[18] S. Jin, Asymptotic preserving (AP) schemes for multiscale kinetic and hyperbolic equations: a review. Lecture Notes for Summer School on "Methods and Models of Kinetic Theory" (M&MKT), Porto Ercole (Grosseto, Italy), June 2010. To appear in Rivista di Matematica della Universita di Parma.
[19] S. Jin and C. D. Levermore, The discrete-ordinate method in diffusive regime, Trans. Theory. Stat. Phys., 20 (1991), 413–439.
[20] S. Y. Kadioglu and M. Sussman, Adaptive solution tecniques for simulating underwater explosions and implosions, J. Comput. Phys., 227 (2008), 2083–2104.
[21] S. Y. Kadioglu, M. Sussman, S. Osher, J. P. Wright and M. Kang, A second order primitive preconditioner for solving all speed multi-phase flows, J. Comput. Phys., 209 (2005), 477–503.
[22] S. Y. Kadioglu, R. Klein and M. L. Minion, A fourth order auxilary variable projection method for zero-Mach number gas dynamics, J. Comput. Phys., 277 (2008), 2012–2043.
[23] S. Klainerman and A. Majda, Singular limits of quasilinear hyperbolic systems with large parameters and the incompressible limit of compressible fluids, Commun. Pure Appl. Math., 34 (1981), 481–524.
[24] R. Klein, Semi-implicit extension of a Godunov-type scheme based on low Mach number asymptotics I: one dimensional flow, J. Comput. Phys., 121 (1995), 213–237.
[25] A. Kurganov and E. Tadmor, New high-resolution central schemes for nonlinear conservation laws and convection-diffusion equations, J. Comput. Phys., 160 (2000), 241–282.
[26] E. W. Larsen and J. E. Morel, Asymptotic solutions of numerical transport problems in optically thick, diffusive regimes II, J. Comput. Phys., 83 (1989), 212–236.
[27] P. D. Lax and X.-D. Liu, Solution of two-dimensional Riemann problems of gas dynamics by positive schemes, SIAM J. Sci. Comput., 19 (1998), 319–340.
[28] J.-G. Liu, J. Liu and R. L. Pego, Stable and accurate pressure approximation for unsteady incompressible viscous flow, J. Comput. Phys., 229 (2010), 3428–3453.
[29] P. Swarztrauber, Fast Poisson solvers, in Studies in Numerical Analysis, ed. G. Golub, AMS, 1984.
[30] R. Temam, Sur l'approximation de la solution des equations de Navier-Stokes par la méthode des fractionnarires II, Arch. Rat. Mech. Anal., 33 (1969), 377–385.
[31] E. Turkel, Preconditioned methods for solving the incompressible and low speed compressible equations, J. Comput. Phys., 72 (1987), 189–209.